Physics Open 13 (2022) 100119

Contents lists available at ScienceDirect

Physics Open

journal homepage: www.sciencedirect.com/journal/physics-open

Doped superior garnet electrolyte toward all-solid-state Li metal batteries

George Xing [a,*], Haoyu Zhu [a], Anna Zhuang [a], Fei Meng [a], Raymond Jiang [a], Shuguang Chen [b], Guanhua Chen [b], Yongchun Tang [a,**]

[a] Power Environmental Energy Research Institute, 738 Arrow Grand Cir, Covina, CA, 91722, USA
[b] Department of Chemistry, The University of Hong Kong, Hong Kong, China

ARTICLE INFO

Keywords:
Cubic phase
Garnet
LLZO
Li-ion
Solid electrolyte

ABSTRACT

$Li_7La_3Zr_2O_{12}$ (LLZO) garnets are one of the most promising solid electrolytes for next generation all-solid-state Li metal batteries due to their high ionic conductivities, chemical stabilities to metallic lithium and wide electrochemical window. Single and co-doped LLZO with Ga, Al, Nb were prepared by solid state reaction and sintered under oxygen atmosphere. Lithium ion conduction properties were investigated through electrochemical impedance spectroscopy in the temperature range of −25 °C–45 °C. Among the doped compositions, Ga doped single phase cubic LLZO shows the highest ionic conductivity of 1.49×10^{-3} S/cm at room temperature and activation energy of 0.27eV, which is one of the best results reported in literature so far in terms of doped garnet structured LLZO. All single or co-doped LLZO samples exhibit low electronic conduction which are 4–5 orders of magnitude lower than their corresponding ionic conductivities. Ga-doped garnet LLZO of high ionic conductivity and negligible electronic conduction makes it a superior solid electrolyte for all-solid-state Li metal batteries.

1. Introduction

Benefited from their high energy and power densities, lithium-ion batteries (LIB) are dominating the battery supply market, especially for the electric vehicles and portable devices [1–4]. However, the conventional LIB uses flammable organic solvent which poses a risk of explosion and fire in the case of leakage, penetration, and consequent overheating [5]. To build a safer LIB, lots of efforts were paid to replace the liquid electrolyte with the nonflammable solid-state electrolyte (SSE) over the last decades [5]. Nevertheless, the ionic conductivity of SSE is still lower than that of common liquid electrolytes, such as LiPF6 in ethylene carbonate (EC)/dimethyl carbonate (DMC) ($\sim 10^{-2}$ S/cm) [6,7]. The researchers have been working on tuning the structures of the SSE to achieve comparable ionic conductivity to and a better overall performance than the liquid electrolyte.

Among all the SSEs, garnet type material has received much scientific attention since the discovery of its high ion conductivity at room temperature [8]. The garnet type SSE also comes with other merits such as the superior thermal and chemical stability, especially the stability against the lithium metal and a wide electrochemical window, which helps realize the direct usage of the lithium metal in the battery to achieve higher energy density and power density [9–11]. In 2007, Murugan et al. first introduced and synthesized cubic lithium stuffed garnet, $Li_7La_3Zr_2O_{12}$ (LLZO) type SSE showing an ionic conductivity of 10^{-4} S/cm [12]. LLZO adopts two crystal structures, cubic (c-LLZO) and tetrahedral (t-LLZO), where the latter one was synthesized in 2009 [13] and found to be the stable structure at room temperature [14,15]. However, the t-LLZO has a significantly lower ionic conductivity than the distorted c-LLZO [12,13]. Thus, the studies to stabilize c-LLZO have been promoted, one possible solution of which is through doping supervalent ions. The Al^{3+} was unintentionally introduced into the c-LLZO from the crucible and found to stabilize the cubic phase efficiently [16]. Soon after, each of the elemental components in the LLZO were substituted by many other elements to engineer this SSE group with higher ionic conductivity and greater stability, which has been summarized in quite a few review articles [5,8,16,17]. Ga^{3+} is so far undoubtedly one of the most successful dopants introduced into the c-LLZO with the Li-ion conductivity around 10^{-3} S/cm at room temperature [6]. But, high cost sintering such as spark plasma sintering, hot pressing etc. are involved in Ga doped LLZO (Ga-LLZO) preparation. Also to enhance Ga-LLZO solid electrolyte density, expensive Pt crucible and unconventional processing such as using chemical cyclohexane to freeze drying Ga-LLZO powder at −20 °C and 60 Pa are employed in Ga-LLZO synthesis. These high cost equipment and unconventional

* Corresponding author.
** Corresponding author.
E-mail addresses: george.xing@peeri.org (G. Xing), tang@peeri.org (Y. Tang).

https://doi.org/10.1016/j.physo.2022.100119
Received 6 June 2022; Received in revised form 16 August 2022; Accepted 25 September 2022
Available online 1 October 2022

processing hindered Ga-LLZO towards commercialization. Here we used conventional tube furnace and low cost alumina crucible by flowing oxygen to prepare high property Ga-LLZO. Another consideration relating to commercialization of LLZO solid electrolyte is doping elements. The cost of Nb_2O_5 is lower than that of Ga_2O_3 which would help limit the cost of the overall LLZO synthesis. Nb_2O_5 has also been reported as an outstanding dopant into LLZO which outperforms most other elements [18]. However, the Nb-doped LLZO (Nb-LLZO) was found to be unstable against the metallic lithium thus not applicable in the practical lithium metal batteries [19]. To address the doping element cost of the Ga-LLZO and the instability of Nb-LLZO, we took a step back and investigated the Al^{3+} doping again as it is in the same group as Ga^{3+} and the very first dopant found to stabilize c-LLZO. The direct comparison between single doped Al-LLZO and Ga-LLZO showed that with the same level of doping, Al-LLZO would be expected to exhibit lower ionic conductivity compared to the Ga-LLZO, which is consistent with previous reports [20]. Here, we proposed co-doping LLZO (AlNb-LLZO) by doping Al^{3+} into A site of LLZO to create cubic phase and doping Nb^{5+} into B site to help maintain the pathway of the Li^{+} migration, Al-LLZO underperforms Ga-LLZO as expected, however the AlNb-LLZO exhibited improvement in terms of ionic conductivity compared to Al-LLZO.

2. Experimental

2.1. Synthesis of LLZO

Three LLZO compositions were prepared by conventional solid-state reaction method. Starting precursors in common among the three powders are $LiOH{\cdot}H_2O$ (battery grade, Alfa Aesar), La_2O_3 (99.99%, Alfa Aesar), ZrO_2 (99.7%, Alfa Aesar), and 10 wt% excess of $LiOH{\cdot}H_2O$ for compensating lithium loss during high temperature processing. Three doping agents were explored in our study: Ga_2O_3 (99.99%, Aldrich) for $Li_{6.4}Ga_{0.2}La_3Zr_2O_{12}$, Al_2O_3 (Standard grade, Aldrich) for $Li_{6.25}Al_{0.25}La_3Zr_2O_{12}$, Al_2O_3 (Standard grade, Aldrich) and Nb_2O_5 (99.99%, Aldrich) for $Li_{6.25}Al_{0.2}La_3Zr_{1.85}Nb_{0.15}O_{12}$. Same processing procedure was applied to all three composition powders. Each powder was mixed with isopropyl alcohol (IPA) and zirconia milling balls in a nylon jar and ball milled at 450 rpm for 6 h. The resulting slurry was put under a fume hood to dry. The air dried powder was fired at 950 °C for 12 h in a covered alumina crucible in order to achieve cubic LLZO phase. The calcined powder was ground with mortar and pestle, and ball milled the second time for 6 h. The resulting mixture was put in a vacuum oven at 80 °C and 76 mmHg for 12 h. The dried powder was sieved using #200 mesh, and 0.7 g of the fine powder was then cold pressed uniaxially into a pellet with diameter $\varphi = 10$ mm under 170Mpa pressure. The pellet with different composition was then covered with its respective mother powder and sintered at 1200 °C for 10 h in a tube furnace with flowing oxygen. Each sintered pellet was polished using 400–1500 grit sandpapers for further characterization.

2.2. Characterization

The relative density of the samples was obtained by measuring the mass and the dimension of the pellets. Sample crystalline phases were measured using X-ray diffraction (XRD) with a Rigaku SmartLab XRD. Colloidal Au paste was applied to both sides of the polished pellets and annealed at 800 °C for an hour. AC impedance measurement was performed in the temperature range of −25 °C–45 °C using a Bio-Logic Science Instruments SAS SP240 potentiostat/galvanostat with frequency range of 0.1 Hz to 7 MHz and amplitude of 10 mV. Total conductivity is calculated using the equation $\sigma = (1/R)(L/A)$, where R is the resistance determined from Nyquist plot, L is the pellet thickness, and A is the pellet area. The electronic conductivity was measured using potentiostatic polarization method. Only electronic conduction presents at steady state because Au blocking electrodes prevent Li-ion from passing. Activation energies for all three composition pellets were calculated using Arrhenius equation based on measured conductivity vs. temperature data.

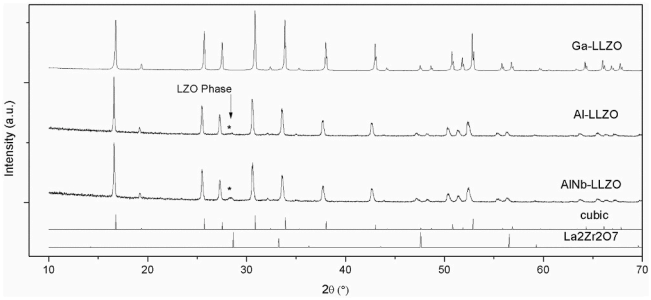

Fig. 1. XRD patterns of Al-LLZO, AlNb-LLZO and Ga-LLZO after calcination, LZO: $La_2Zr_2O_7$.

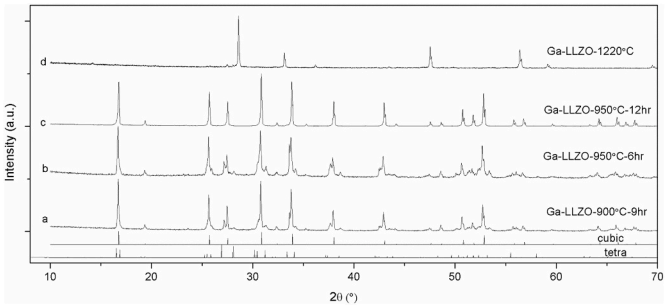

Fig. 2. XRD patterns of Ga-LLZO phase evolution after annealed under different conditions.

3. Results and discussion

3.1. Structural analysis and phase evolution

Fig. 1 shows the XRD diffraction patterns of Ga, Al and Nb in single or co-doped LLZO garnet samples after calcination at 950 °C in air. All diffraction patterns of the samples with nominal compositions $Li_{6.4}Ga_{0.20}La_3Zr_2O_{12}$ (Ga-LLZO), $Li_{6.25}Al_{0.25}La_3Zr_2O_{12}$ (Al-LLZO) and $Li_{6.25}Al_{0.20}La_3Zr_{1.85}Nb_{0.15}O_{12}$ (AlNb-LLZO) were indexed to cubic symmetry with the space group *Ia*-3d. However, we observed a trace amount of pyrochlore phase $La_2Zr_2O_7$ (LZO) impurity in Al-LLZO and AlNb-LLZO compositions. The LZO phase was initially formed from precursors of La_2O_3 and ZrO_2 at the temperature around 790 °C by solid state reactions. With the temperature increasing above 900 °C, melted LiOH and doping compounds were incorporated into LZO and formed garnet structured LLZO in the mixture of tetragonal and cubic phases. The tetragonal phase forms preferentially over the cubic phase due to its thermodynamic stability at this temperature. Further calcination at higher temperature, the garnet LLZO converts from tetragonal to cubic phase. It has been reported that lithium in cubic LLZO is significantly less than in tetragonal phase [21,22]. Shimonishi et al. reported tetragonal LLZO having 7 and 7.5 lithium ions per formula unit but only 6.0 lithium ions in cubic phase indicating Li concentration and its high temperature evaporation is critical to LLZO cubic phase formation [23]. LZO impurity phase was also formed when lithium in cubic phase LLZO was over evaporated during high temperature calcination or sintering. Fig. 2 shows the phase evolution of LLZO powders calcined in air. Shoulder peaks observed in Fig. 2 (a, b) confirms cubic and tetragonal phases coexistence in LLZO after calcination at 900 °C for 9 h and 950 °C for 6 h respectively. Further calcination at 950 °C for an extra 6 h resulted in a phase transformation from tetragonal to pure cubic LLZO as shown in Fig. 2c. When high temperature processing was performed

Table 1
Literature result of Ga doped LLZO ionic conductivity at 25 °C.

Composition	Relative density %	σtotal S/cm	Ea Ev	σelectronic S/cm	Ref.
$La_{6.4}Ga_{0.2}La_3Zr_2O_{12}$	93	1.49×10^{-3}	0.27		This work
$La_{6.55}Ga_{0.15}La_3Zr_2O_{12}$	–	1.0×10^{-3}	–	–	
$La_{6.4}Ga_{0.2}La_3Zr_2O_{12}$	97	9.4×10^{-4}	0.33	4.3×10^{-8}	37
$La_{6.4}Ga_{0.2}La_3Zr_2O_{12}$	–	1.0×10^{-3}	0.30	5.0×10^{-10}	38
$La_{6.4}Ga_{0.2}La_3Zr_2O_{12}$	–	1.32×10^{-3}	0.26	–	39
$La_{6.4}Ga_{0.2}La_3Zr_2O_{12}$	97	1.24×10^{-3}	0.31	5.04×10^{-8}	37
$La_{6.25}Ga_{0.25}La_3Zr_2O_{12}$	91	3.5×10^{-4}	–	7.1×10^{-8}	40
$La_{6.25}Ga_{0.25}La_3Zr_2O_{12}$	94	1.46×10^{-3}	0.25	5.4×10^{-8}	34
$La_{6.25}Ga_{0.25}La_3Zr_2O_{12}$	98	1.48×10^{-3}	0.27	–	41
$La_{6.25}Ga_{0.25}La_3Zr_2O_{12}$	93	6.5×10^{-4}	0.27	–	41

over a long period, the cubic phase started to decompose as a result of lithium loss and the LZO phase was formed again (as seen in Fig. 2d), which is consistent with literature reports [21,24]. Based on the above phase evolution, we fixed the calcination condition as 950 °C for 12 h.

3.2. Doping strategy and garnet framework

The cubic phase LLZO shows a Li-ion conductivity of 10^{-3}–10^{-4} S/cm at room temperature, which is two orders of magnitudes higher than that of the tetragonal phase. However, the cubic phase is not stable at room temperature [25]. Therefore, supervalent cations are introduced to stabilize high conductivity cubic LLZO garnet structure. Supervalent doping also functions to create the Li-ion vacancies through charge compensation and reduce the degree of Li-ion local ordering. We chose Al^{3+} as LLZO dopant mainly because its raw material cost is low. Al^{3+} is believed to create Li-ion vacancies and stabilize cubic LLZO phase, but doped Al^{3+} occupies on Li-ion sites and thus blocks Li-ions transport channels and affects Li-ion conductivity. Therefore, conductivities of Al^{3+} doped LLZO are relatively low. As mentioned above, the XRD diffraction pattern for the nominal composition of $Li_{6.25}Al_{0.25}La_3Zr_2O_{12}$ (Al-LLZO) shows a cubic phase with a small amount of LZO impurity (Fig. 1), which may be another factor of lower conductivity of the Al-LLZO. Our AC impedance measurement shows Al-LLZO solid electrolyte conductivity of 2.7×10^{-4} S/cm at room temperature, which is consistent with the literature reports of 1.4–2.5 $\times$ 10^{-4} S/cm [23, 26–29].

In co-doping of AlNb-LLZO, a first dopant cation Al^{3+} is introduced into the LLZO garnet framework and occupies Li-ion 24d sites to stabilize the LLZO cubic phase, in the meantime, a second cation Nb^{5+} provides partially substitution of the Zr at 16a sites to reduce Li-ion content and increase the concentration of Li-ions vacancies by charge compensation [30–32]. Similar ionic radii for Nb^{5+} of 64 p.m. and Zr^{4+} of 72 p.m. make this partial substitution feasible. Shingo Ohta et al. reported Nb^{5+} doped LLZO has the total conductivity of 8×10^{-4} S/cm for $Li_{6.75}La_3Zr_{1.75}Nb_{0.25}O_{12}$ garnet [29]. Although different doping levels of Nb^{5+} were introduced into LLZO garnet and some of them involved the adventitious Al^{3+} from alumina crucible via chemical diffusion during high temperature processing [22,23], we have not seen a literature report about co-doping of LLZO with Nb^{5+} and Al^{3+} cations by conventional solid state reaction. Here we report a co-doped garnet electrolyte with nominal composition of $Li_{6.25}Al_{0.20}La_3Zr_{1.85}Nb_{0.15}O_{12}$ prepared via solid state route and measured conductivity of 3.9×10^{-4} S/cm at room temperature.

LLZO garnet stabilized with Ga^{3+} shows obviously superior properties compared to LLZO stabilized with similar cations. Ga^{3+} doped LLZO confirms over two times higher lithium conductivity over the Al^{3+} doped LLZO. The supervalents Ga^{3+} and Al^{3+} have site preference in LLZO lithium substitution. The larger cation Ga^{3+}(62pm) prefers the 96 h site, which is less hindering for long-range Li-ion transport compared to Al^{3+}(53pm) occupying at the 24d site, a junction for Li-ion diffusion [33]. It is generally agreed that in the cubic LLZO garnet framework, the Li-ions occupy the three different positions: tetrahedral 24d site, octahedral 48 g, and distorted octahedral 96 h with 96 h site Li-ions exhibiting the highest mobility. The 3 sites Li-ions combine forming a continuous 3D network of moving Li^+ ions in the interstitial space of the 3D garnet framework. According to literature, there are two transport pathways: 96 h–96 h and 24d-96 h-24d, but the 96 h–96 h pathway determines the overall conductivity [34]. Goodenough et al. [35] reported that the best Li^+ concentration in $Li_{7-x}La_3Zr_{2-x}Ta_xO_{12}$ garnet for Li^+ transport is in the range $6.4 \leq x \leq 6.6$, which is consistent with the Li^+ concentration of $X_{Li} = 6.4$ for the nominal composition of $Li_{6.4}Ga_{0.20}La_3Zr_2O_{12}$ in our Ga-LLZO. By optimizing the unique properties of Ga^{3+} doped LLZO framework, high Li-ion conductivity of 1.49 $\times$ 10^{-3} S/cm Ga-LLZO garnet electrolyte was successfully prepared by solid state reaction, which shows one of the best ionic conductivity reported by literature (see Table 1). This superior Ga-LLZO garnet electrolyte allows high capacity Li metal as anode and is one step further toward next generation all-solid-state Li metal batteries commercialization.

3.3. Electrical analysis

Fig. 3a shows a typical Nyquist plot for a nominal composition of $Li_{6.55}Ga_{0.15}La_3Zr_2O_{12}$ solid electrolyte pellet bonded with Au paste as blocking electrodes (Fig. 3b) for Li-ion conductivity measurements. The Au paste was applied and sintered at 800 °C to form good bonding with the pellet. The equivalent circuit can be represented as: R1+R2/

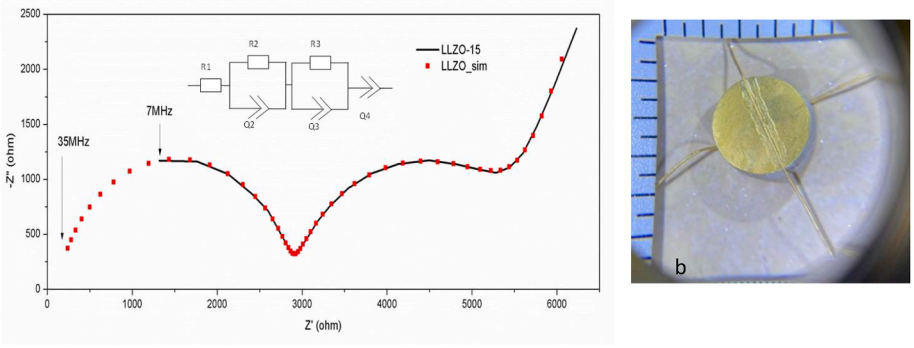

Fig. 3. (a) Typical AC impedance spectra of $Li_{6.55}Ga_{0.15}La_3Zr_2O_{12}$ (x = 0.15) at 25 °C, (b) The pellet bonded with Au paste as blocking electrodes.

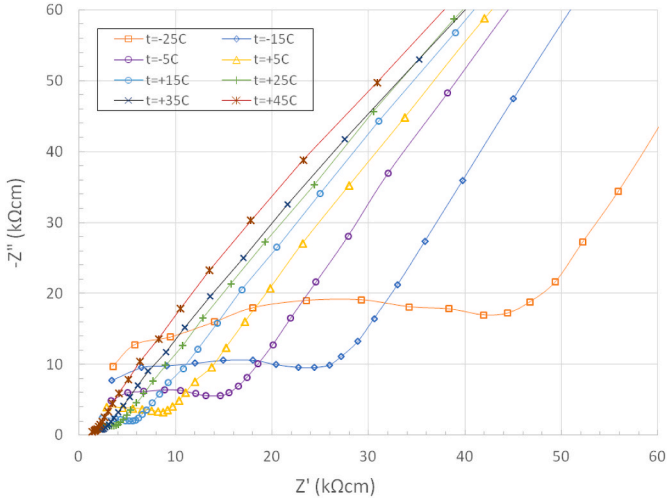

Fig. 4. AC impedance spectra of Al-LLZO pellet at temperatures between −25 °C and 45 °C.

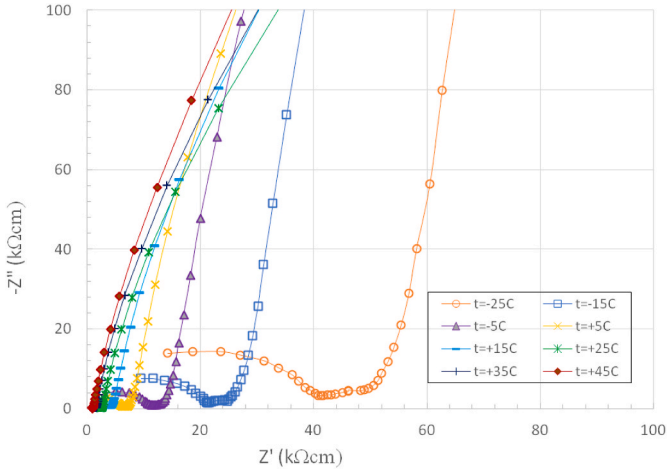

Fig. 5. AC impedance spectra of AlNb-LLZO pellet at temperatures between −25 °C and 45 °C.

Q2+R3/Q3+Q4 where Q refers to constant phase element and R1, ohmic resistance, R2, bulk resistance, Q2, bulk capacitance, R3, grain boundary resistance, Q3, grain boundary capacitance, Q4, dispersive line respectively. The two depressed semicircles at high-medium frequencies in the spectrum are associated with the bulk and grain boundary processes respectively. The about 45° dispersive line at low frequencies is the result of Li-ion transport being blocked by the Au electrode. Only part of the high frequency semicircle is presented due to our AC impedance unit peak frequency limitation. However, a complete semicircle can be achieved through equivalent circuit modeling when the fitting frequency is extended up to 35 MHz. The impedance spectra of single element doped Al-LLZO at different temperatures is shown in Fig. 4. Different from the typical Nyquist plot in Fig. 3a, the bulk semicircle and grain boundary semicircle cannot be deconvoluted even at low temperature of −25 °C as only one semicircle is observed in high frequencies. With temperature increasing, the semicircle diameter decreases. A spike in low frequencies is also observed. The equivalent circuit of R1+R2/Q2+Q3 is chosen to fit the plot. Considering the pellet sample geometry, the total conductivity is calculated as 4.0×10^{-5} S/cm at −15 °C. Literature reported when grain boundaries are comparable to or more conductive than the bulk, the impedance spectra cannot be readily deconvoluted. In this situation the corresponding capacitances of the semicircles for bulk and grain boundary overlap each other. One

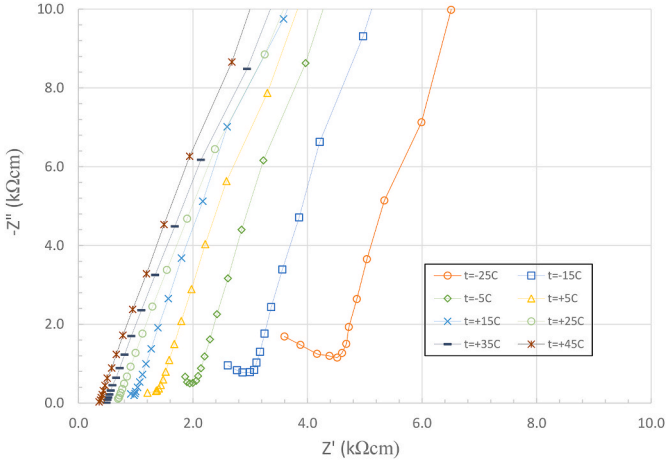

Fig. 6. AC impedance spectra of Ga-LLZO pellet at temperatures between −25 °C and 45 °C.

possible approach of separating them is to grow a single crystal according to the compositions of the grain and grain boundary then perform corresponding impedance measurements to determine each conductivity.

Co-doped AlNb-LLZO Nyquist plot is shown in Fig. 5. The two semicircles are clearly separated at all testing temperatures. The equivalent circuit can be expressed as R1/Q1+R2/Q2+Q3. The capacitance (Q1) associated with the high frequent semicircle is on the levels of 10^{-10}–10^{-9} F indicating a bulk contribution and the low frequency capacitance (Q2) ranging from 10^{-5}–10^{-4} F is ascribed to grain boundary effect [36]. A total conductivity of 4.9×10^{-5} S/cm at −15 °C is obtained in which the bulk conductivity is 4.6×10^{-5} S/cm and grain boundary conductivity is 2.9×10^{-5} S/cm.

The Nyquist plot of Ga-LLZO for the nominal composition of $Li_{6.4}Ga_{0.20}La_3Zr_2O_{12}$ is presented in Fig. 6. Two different types of spectra are displayed with testing temperatures varying. When the Ga-LLZO pellet sample is tested at low temperatures from −25 °C to 5 °C, the high frequency semicircle with dispersive lines in low frequencies are seen in the spectrum. With the temperature increasing, the semicircle diameters decrease until they totally vanish at above 5 °C. In the temperature range of 15–45 °C, only dispersive lines are observed. With the equivalent circuit of R1/Q1+Q2, the total conductivity is calculated at −15 °C of 3.2×10^{-4} S/cm. Table 1 lists literature results for Ga doped LLZO total conductivity at 25 °C. Our optimized Ga doped LLZO garnet exhibits one of the best results among reported conductivities in recent years.

All solid electrolyte pellet samples for Li-ion conductivity measurements have relative density above 92%. Fig. 7 presents scanning electron microscope (SEM) images of cross-section of Ga-LLZO sample sintered in oxygen atmosphere. The average grain size was estimated to be 5–20 μm according to Fig. 7a. Further observation from higher magnification SEM indicated the grains were fully sintered together (Fig. 7b). Flowing oxygen helped to expel the pores out of grains and grain boundaries leading to density enhancement. High density reduced intergrain ionic resistance and led to higher ionic conductivity of the material given higher density provided more pathways for Li-ions transport across the material. Thus, high density was a key factor for the Ga-LLZO to achieve superior electrical properties. Fig. 8 shows the Arrhenius plot of the Li-ion conductivity versus 1000/T for single and co-doped LLZO samples Ga-LLZO, Al-LLZO and AlNb-LLZO in the temperature range from −25 °C to 45 °C. The activation energy (Ea) can be estimated according to the Arrhenius equation

$$\sigma T = A exp(\frac{E_a}{kT})$$

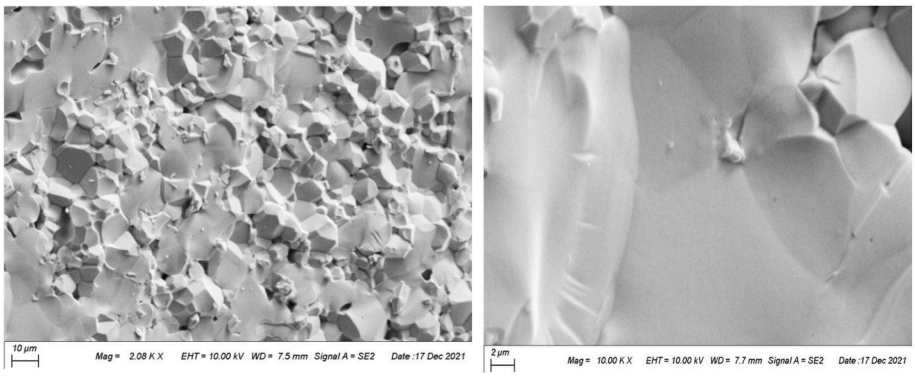

Fig. 7. SEM cross-section of oxygen-sintered Ga-LLZO; a) x2,000, b) x10,000.

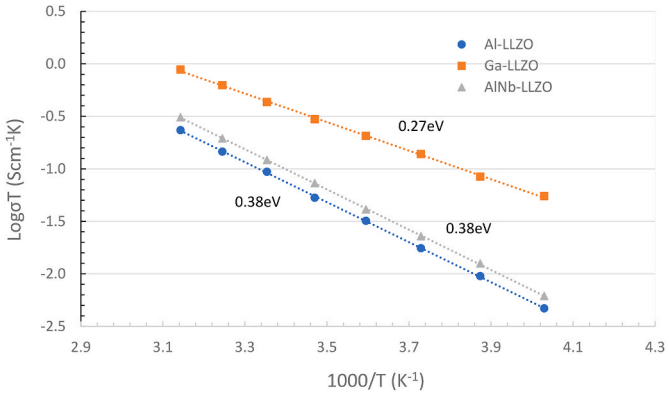

Fig. 8. Arrhenius plot of Al-LLZO, AlNb-LLZO and Ga-LLZO pellets with Au paste as blocking electrodes in the temperature range of −25 °C–45 °C.

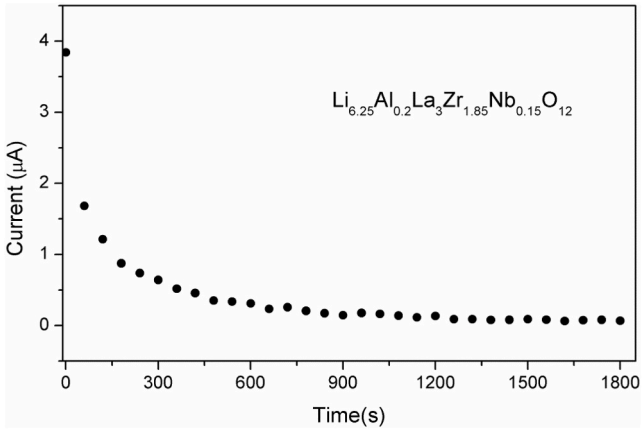

Fig. 9. Electronic conductivity measurements for doped LLZO.

Table 2
Total conductivity, electronic conductivity, transference number and relative density of pellet samples.

Samples	σ_total (mS/cm)	σ_electronic (10^{-8}S/cm)	t_{Li}	Relative density %
$Li_{6.25}Al_{0.2}La_3Zr_{1.85}Nb_{0.15}O_{12}$	0.39	1.80	1	95
$Li_{6.4}Al_{l0.2}La_3Zr_2O_{12}$	0.27	0.12	1	92
$Li_{6.4}Ga_{0.2}La_3Zr_2O_{12}$	1.49	1.20	1	93

where σ is total Li-ion conductivity, A the pre-exponential factor, k the Boltzmann constant and T the absolute temperature. The Ga-LLZO gives the lowest activation energy of 0.27eV and the highest Li-ion conductivity among the three solid state electrolytes, which is possible to be ascribed to the enhanced mobility of lithium ions arising from the coulombic repulsion between Ga^{3+} and Li^{+} ions. Both Al-LLZO and AlNb-LLZO have the same activation energy of 0.38eV but AlNb-LLZO shows slightly higher Li-ion conductivity.

The steady state current plot under applied voltage was recorded through chronoamperometry measurement, as shown in Fig. 9 for an Al and Nb co-doped LLZO sample. Table 2 lists the electronic conductivities of several samples that were calculated taking into account their thickness and diameter. The typical electronic conductivity values lie in the order of 10^{-8} S/cm, which is several orders of magnitude lower than the total electrical conductivity measured using electrochemical impedance spectroscopy. This indicates the transference number of Lithium ions is very close to unity, as indicated in Table 2.

4. Conclusions

In summary, single doping or co-doping strategies are introduced into garnet LLZO syntheses to stabilize cubic phase and promote Li-ion conductivity. High density (>92%) solid electrolytes were prepared by conventional solid-state reactions under oxygen flowing in the sintering processing. Electrical properties of Ga-LLZO, Al-LLZO and AlNb-LLZO solid electrolytes investigated using electrochemical impedance spectroscopy technique in the temperature range of −25 °C–45 °C show Ga doped single phase garnet Ga-LLZO has the highest ionic conductivity of 1.49×10^{-3} S/cm at room temperature and activation energy of 0.27eV. Coulombic repulsion between Ga^{3+} and Li^{+} generating more high mobility 96 h sites Li-ions is considered to be a vital factor for the high conductivity. Al-LLZO and AlNb-LLZO have the same activation energy of 0.38eV but AlNb-LLZO shows slightly higher Li-ion conductivity than that of Al-LLZO. All single or co-doped LLZO samples exhibit low electronic conduction which are 4–5 orders of magnitude lower than their corresponding ionic conductivities.

CRediT authorship contribution statement

Haoyu Zhu: Investigation, Writing – original draft. **Anna Zhuang:** Investigation, Writing – original draft. **Fei Meng:** Investigation. **Raymond Jiang:** Investigation. **Shuguang Chen:** Project administration. **Guanhua Chen:** Project administration. **Yongchun Tang:** Supervision.

Declaration of competing interest

The authors declare that they have no known competing financial interests or personal relationships that could have appeared to influence the work reported in this paper.

Acknowledgments

The authors would like to thank the Hong Kong Quantum AI Lab Limited for their support. Prof. William Goddard III at California Institute of Technology is gratefully acknowledged for assisting with our instrumentation.

References

[1] M. Armand, J.M. Tarascon, Building better batteries, Nature 451 (2008) 652–657.
[2] S. Chu, A. Majumdar, Opportunities and challenges for a sustainable energy future, Nature 488 (2012) 294–303.
[3] G.E. Blomgren, The development and future of lithium ion batteries, J. Electrochem. Soc. 164 (2016) A5019–A5025.
[4] M. Li, J. Lu, Z. Chen, K. Amine, 30 Years of lithium-ion batteries, Adv. Mater. 30 (2018), 1800561.
[5] C. Sun, J. Liu, Y. Gong, D.P. Wilkinson, Zhang, Recent advances in all-solid-state rechargeable lithium batteries, J., Nano Energy 33 (2017) 363–386.
[6] S. Qin, X. Zhu, Y. Jiang, M.e. Ling, Z. Hu, Zhu, Growth of self-textured Ga3+-substituted Li7La3Zr2O12 ceramics by solid state reaction and their significant enhancement in ionic conductivity, J., Applied Physics Letters 112 (2018), 113901.
[7] M. Schmidt, U. Heider, A. Kuehner, R. Oesten, M. Jungnitz, N. Ignat'ev, P. Sartori, Lithium fluoroalkylphosphates: a new class of conducting salts for electrolytes for high energy lithium-iron batteries, J. Power Sources 97 (2001) 557.
[8] A. Kim, S. Woo, M. Kang, H. Park, B. Kang, Research progresses of garnet-type solid electrolytes for developing all-solid-state Li batteries, Front. Chem. 8 (2020) 468.
[9] V. Thangadurai, D. Pinzaru, S. Narayanan, A.K. Baral, Fast solid-state Li ion conducting garnet-type structure metal oxides for energy storage, J. Phys. Chem. Lett. 6 (2015) 292–299.
[10] K. Hofstetter, A.J. Samson, S. Narayanan, V. Thangadurai, Present understanding of the stability of Li-stuffed garnets with moisture, carbon dioxide, and metallic lithium, J. Power Sources 390 (2018) 297–312.
[11] H. Duan, H. Zheng, Y. Zhou, B. Xu, H. Liu, Stability of garnet-type Li ion conductors: an overview, Solid State Ionics 318 (2018) 45–53.
[12] R. Murugan, V. Thangadurai, W. Weppner, Fast lithium ion conduction in garnet-type $Li_7La_3Zr_2O_{12}$, Angew. Chem. Int. Ed. 46 (2007) 7778–7781.
[13] J. Awaka, N. Kijima, H. Hayakawa, Akimoto, Synthesis and structure analysis of tetragonal $Li_7La_3Zr_2O_{12}$ with the garnet-related type structure, Journal of Solid State Chemistry France 182 (2009) 2046.
[14] A. Logéat, T. Köhler, U. Eisele, B. Stiaszny, A. Harzer, M. Tovar, A. Senyshyn, H. Ehrenberg, B. Kozinsky, From order to disorder: the structure of lithium-conducting garnets Li_7 – xLa3TaxZr2 – xO12 (x= 0–2), Solid State Ionics 206 (2016) 33–38.
[15] I. Quinzeni, D. Capsoni, V. Berbenni, P. Mustarelli, M. Sturini, M. Bini, Stability of low-temperature $Li_7La_3Zr_2O_{12}$ cubic phase: the role of temperature and atmosphere, Mater. Chem. Phys. 185 (2017) 55–64.
[16] A.J. Samson, K. Hofstetter, S. Bag, V. Thangadurai, A bird's-eye view of Li-stuffed garnet-type $Li_7La_3Zr_2O_{12}$ ceramic electrolytes for advanced all-solid-state Li batteries, Energy Environ. Sci. 12 (2019) 2957–2975.
[17] P. Verma, P. Maire, P. Novák, A review of the features and analyses of the solid electrolyte interphase in Li-ion batteries, Electrochim. Acta 55 (2010) 6332–6341.
[18] V. Thangadurai, H. Kaack, W.J.F. Weppner, Novel fast lithium ion conduction in garnet-type Li5La3M2O12 (M: Nb, Ta), J. Am. Ceram. Soc. 86 (2003) 437.
[19] M. Nakayama, M. Kotobuki, H. Munakata, M. Nogami, K. Kanamura, First-principles density functional calculation of electrochemical stability of fast Li ion conducting garnet-type oxides, Phys. Chem. Chem. Phys. 14 (2012), 10008.
[20] G. Han, B. Kinzer, R. Garcia-Mendez, H. Choe, J. Wolfenstine, Sakamoto, Correlating the effect of dopant type (Al, Ga, Ta) on the mechanical and electrical properties of hot-pressed Li-garnet electrolyte, J, J. Eur. Ceram. Soc. 40 (2020) 1999.
[21] Ezhiyl Rangasamy, Jeff Wolfenstine, Jeffrey Sakamoto, The role of Al and Li concentration on the formation of cubic garnet solid electrolyte of nominal composition $Li_7La_3Zr_2O_{12}$, Solid State Ionics 206 (2012) 28–32.
[22] C.A. Geiger, E. Alekseev, B. Lazic, M. Fisch, T. Armbruster, R. Langner, Crystal chemistry and stability of $Li_7La_3Zr_2O_{12}$ garnet: a fast lithium-ion conductor, Inorg. Chem. 50 (2011) 1089–1097.
[23] Y. Shimonishi, A. Toda, T. Zhang, A. Hirano, N. Imanishi, O. Yamamoto, Y. Takeda, Synthesis of garnet-type $Li_{7-x}La_3Zr_2O_{12-1/2x}$ and its stability in aqueous solutions, Solid State Ionics 183 (2011) 48.
[24] M. Huang, T. Liu, C. Nan, Effect of sintering temperature on structure and ionic conductivity of $Li_{7-x}La_3Zr_2O_{12-0.5x}$ (x=0.5~0.7) ceramics, Solid State Ionics 204 (2011) 41–45.
[25] H. Buschmann, et al., Structure and dynamics of the fast lithium ion conductor $Li_7La_3Zr_2O_{12}$, Physiol. Chem. Phys. 13 (2011) 19378–19392.
[26] M. Kotobuki, H. Munakata, K. Kanamura, Y. Sato, T. Yoshida, Compatibility of $Li_7La_3Zr_2O_{12}$ solid electrolyte to all-solid-state battery using Li metal anode, J. Electrochem. Soc. 157 (2010). A1076.
[27] S. Kumazaki, Y. Iriyama, K.-H. Kim, R. Murugan, K. Tanabe, K. Yamamoto, T. Hirayama, R. Murugan, Z. Ogumi, High lithium ion conductive $Li_7La_3Zr_2O_{12}$ by inclusion of both Al and Si, Electrochem. Commun. 13 (2011) 509–512.
[28] K.-H. Kim, Y. Iriyama, K. Yamamato, S. Kumazaki, T. Asaka, K. Tanabe, C.A. J. Fisher, T. Hirayama, R. Murugan, Z. Ogumi, Characterization of the interface between $LiCoO_2$ and $Li_7La_3Zr_2O_{12}$ in an all-solid-state rechargeable lithium battery, J. Power Sources 196 (2011) 764–767.
[29] S. Ohta, T. Kobayashi, T. Asaoka, High lithium ionic conductivity in the garnet-type oxide $Li_{7-X}La_3(Zr_{2-X}, Nb_X)O_{12}$ (X = 0–2), J. Power Sources 196 (2011) 3342–3345.
[30] V. Thangadurai, S. Narayanan, D. Pinzaru, Garnet-type solid- state fast Li ion conductors for Li batteries: critical review, Chem. Soc. Rev. 43 (2014) 4714–4727.
[31] C. Cao, Z.-B. Li, X.-L. Wang, X.-B. Zhao, W.-Q. Han, Recent advances in inorganic solid electrolytes for lithium batteries, Front. Energy Res. 2 (2014) 25.
[32] R.D. Shannon, C.T. Prewitt, Effective ionic radii in oxides and fluorides, Acta Crystallogr. Sect. B Struct. Crystallogr. Cryst. Chem. 25 (1969) 925–946.
[33] J.L. Allen, J. Wolfenstine, E. Rangasamy, J. Sakamoto, Effect of substitution (Ta, Al, Ga) on the conductivity of $Li_7La_3Zr_2O_{12}$, J. Power Sources 206 (2012) 315–319.
[34] J.-F. Wu, E.-Y. Chen, Y. Yu, L. Liu, Y. Wu, W.K. Pang, V.K. Peterson, X. Guo, Gallium-doped $Li_7La_3Zr_2O_{12}$ garnet-type electrolytes with high lithium-ion conductivity, ACS Appl. Mater. Interfaces 9 (2017) 1542–1552.
[35] Yutao Li, Jian-Tao Han, Chang-An Wang, Hui Xie, John B. Goodenough, Optimizing Li+ conductivity in a granet framework, J. Mater. Chem. 22 (2012), 15357.
[36] John T.S. Irvine, Derek C. Sinclair, Anthony R. West, Electroceramics : characterization by impedance spectroscopy, Adv. Mater. 2 (1990) 132–138.
[37] Jianmeng Su, Xiao Huang, Zhen Song, Tongping Xiu, Michael E. Badding, Jun Jin, Zhaoyin Wen, Overcoming the abnormal grain growth in Ga-doped $Li_7La_3Zr_2O_{12}$ to enhance the electrochemical stability against Li metal, Ceram. Int. 45 (2019) 14991–14996.
[38] M. Philipp, B. Gadermaier, P. Posch, I. Hanzu, S. Ganschow, M. Meven, D. Rettenwander, G.J. Redhammer, H.M.R. Wilkening, The electronic conductivity of single crystalline Ga-stabilized cubic $Li_7La_3Zr_2O_{12}$: a technologically relevant parameter for all-solid-state batteries, Adv. Mater. Interfac. 7 (2020), 2000450.
[39] D. Rettenwander, G. Redhammer, F. Preishuber-Pflügl, L. Cheng, L. Miara, R. Wagner, A. Welzl, E. Suard, M.M. Doeff, M. Wilkening, J. Fleig, G. Amthauer, Structural and electrochemical consequences of Al and Ga Co-substitution in $Li_7La_3Zr_2O_{12}$ solid electrolytes, Chem. Mater. 28 (2016) 2384–2392.
[40] J. Wolfenstine, J. Ratchford, E. Rangasamy, J. Sakamoto, J.L. Allen, Synthesis and high Li-ion conductivity of Ga-stabilized cubic $Li_7La_3Zr_2O_{12}$, Mater. Chem. Phys. 134 (2012) 571–575.
[41] Xiaomei Zenga, Andrew J. Martinolichb, Kimberly A. Seeb, Katherine T. Faber, Dense garnet-type electrolyte with coarse grains for improved air stability and ionic conductivity, J. Energy Storage 27 (2020), 101128.